Wear Resistance of Spark Ignition Engine Piston Rings in Hydrogen-Containing Environments

Myroslav Kindrachuk [1], Dmytro Volchenko [2], Alexander Balitskii [3,4,*], Karol F. Abramek [4], Mykola Volchenko [5], Olexiy Balitskii [6], Vasyl Skrypnyk [2], Dmytro Zhuravlev [7], Alina Yurchuk [1] and Valerii Kolesnikov [3,8]

1 Aerospace Faculty, National Aviation University, 03-058 Kyiv, Ukraine; nau12@ukr.net (M.K.); alina20182017@gmail.com (A.Y.)
2 Institute of Petroleum Engineering, Ivano-Frankivsk National Technical University of Oil and Gas, 76-000 Ivano-Frankivsk, Ukraine; vol21@ukr.net (D.V.); skripnik-vs07@ukr.net (V.S.)
3 Department of Strength of the Materials and Structures in Hydrogen-Containing Environments, Karpenko Physico-Mechanical Institute, National Academy of Sciences of Ukraine, 79-601 Lviv, Ukraine; kolesnikov197612@gmail.com
4 Department of Automotive Engineering, West Pomeranian University of Technology in Szczecin, 70-310 Szczecin, Poland; karol.abramek@zut.edu.pl
5 Institute of Mechanics, Robotics, Engineering of Transport and Technical Systems, Ivano-Frankivsk National Technical University of Oil and Gas, 76-000 Ivano-Frankivsk, Ukraine; volchenko.nik@yandex.ru
6 Department of System Design, Lviv Ivan Franko National University, 79-005 Lviv, Ukraine; olexiybal@yahoo.com
7 Institute of Mechanical Engineering, Ivano-Frankivsk National Technical University of Oil and Gas, 76-000 Ivano-Frankivsk, Ukraine; dmytro.2103@ukr.net
8 Department of Production Technology and Professional Education, Taras Shevchenko National University of Lugansk, 92-703 Starobilsk, Ukraine
* Correspondence: balitski@ipm.lviv.ua or abalicki@zut.edu.pl

Abstract: We describe the external and internal hydrogen interaction on contacting surfaces in the "cylinder–piston rings" friction coupling. Under the influence of high temperatures and pressure, the oil in the combustion chamber at a temperature up to 1473 K decomposes and forms small amounts of water. External hydrogen (H_2) is subsequently formed. Hydrogen removal from the piston rings reduces the heterogeneity of the structure, residual stresses, and uneven physical and chemical properties of the near-surface layers, which reduces the stress concentration and, as a consequence, results in an improvement in the performance characteristics of the surface layers of the friction couple "cylinder-piston rings" of the spark ignition engine.

Keywords: spark-ignition engine; cylinder–piston ring friction couple; external and internal hydrogen; hydrogen wear; wear resistance of materials; energy levels; hydrogen intercalation

1. Introduction, State of the Art, and Problem Formulation

When the friction coupled "cylinder–piston ring" moves, there is a cyclic change in alternating loads at high temperatures up to 3000 K and specific loads—10–12 MPa in the diesel engines and up to 5.5 MPa in the spark-ignition motors. These operating conditions lead to the thermomechanical destruction of fuel and oil combustion products by forming free (external) hydrogen and its subsequent adsorption by the rubbing surfaces. The periodic occurrence of alternating stress waves (tension–compression) enhances the saturation of near-surface metal volumes by hydrogen during friction and cavitation [1–7], and these phenomena using experimental equipment [1,2].

The obtained results show that the piston rings of D-50, D-240, ZMZ-24, CC-10UD, and other engines are mainly subjected to both technological and operational hydrogen saturation, causing their embrittlement. This process contributes to intensive wear [2–10]. Authors [6–21] have analyzed the features of hydrogen wear of construction machine parts.

The general laws of hydrogen wear are considered a specific type of surface crack initiation and destruction. The ways of surface hydrogenation are established, the mechanism of hydrogen wear of machine parts and equipment is discussed, and the methods of protection against tribohydrogen saturation are formulated [10]. On the other hand, the interaction of hydrogen with metals and non-metallic elements [19–23] and its influence on various properties of metals, alloys, hydrogen-induced specific defects, and hydrogen embrittlement, as well as the effect of hydrogen on the mechanical characteristics in the "hydrogen–metal" couple, are assessed [1,2,10].

During the cavitation and wear of the sub-roughness of friction surfaces in a hydrogen-containing environment [1,9], hydrogen is pumped into the subsurface layer of the metal and interacts with its crystal lattice. It is noted that the driving forces in the processes of hydrogen wear are temperature, pressure, deformation, structure, and crystal lattice defects. The physical and mechanical processes on the friction surface of the hydrogen wear of machine and equipment parts are investigated, and the reasons for the release of hydrogen–hydrogen absorption by rubbing surfaces and their destruction have been established [6–10].

A complex picture of hydrogen behavior in surface layers during friction under the influence of various factors is shown, and the impact of "biographical" hydrogen on the wear of parts is determined. Practical recommendations are relevant for suppressing hydrogen wear and increasing the durability and reliability of friction units of machines and equipment. In this case, the following are not considered: the effect of external hydrogen on the surface layer of the metal friction element and its entry into the subsurface layer by "pumping"; the phenomenon of adhesion and the types of contacts of friction couples; and the combination of adsorption, diffusion phenomena observed in the surface, and subsurface layers of friction couples. Most importantly, there was no approach to external and internal hydrogen and its role in tribological reactions.

This paper addresses the following issues concerning the problem being solved: the interaction of external and internal hydrogen in a "cylinder–piston rings" friction couple, and the hydrogen wear of the piston rings of engine cylinders and ways to reduce it. This work aims to establish the relationship between technological (internal) and operational (external) hydrogen in piston engine cylinder wear.

2. Interaction of External and Internal Hydrogen in "Cylinder–Piston Ring" Friction Couple

Spark ignition engines are the most common heat engines in the world today. The central working unit of such engines is a piston, along the height of which compression and oil-retaining rings are set in the grooves. During engine operation, uneven wear of the piston rings occurs due to the different work of friction, specific loads, and energy loading caused by exposure to hot exhaust gases. Hydrogen in the fuel and lubricant contributes to the piston rings' wear due to atomic hydrogen [1–6,16].

Hydrogen wear of the rings can occur in several different pathways. One of them is the interaction of the rings with internal and external hydrogen. During electrothermomechanical [12–15] friction, external hydrogen is released from the fuel and lubricant. Then, through a recombination reaction, molecular hydrogen transforms into atomic hydrogen as $H_2 \leftrightarrow 2H$. Under the concentration gradients, surface and volumetric temperature, and pressure, hydrogen diffuses to the zone of its lowest concentration, highest temperature, and lowest pressure. In this case, its diffusivity depends on the metal structure, the presence of alloying elements, and the defectiveness of the crystal lattice. In addition, friction creates an electromagnetic field, which drifts external charged hydrogen into microcracks.

External hydrogen from the fuel and lubricant during friction is also accompanied by nitrogen and oxygen desorbed from the metal. The latter interacts with the metal surface, where a temperature gradient exists. Those gradients between the external and internal hydrogen, vacancies, and other defects in the crystal lattice lead to the formation of zones in which the external hydrogen is introduced. Thus, the external hydrogen "pushes" the internal hydrogen, and desorption plays a vital role in the hydrogen wear process.

During electrothermomechanical friction [12–14], the micro-roughness of the rings undergoes plastic and elastic deformation. The latter, slightly changing the unit cell volume, facilitates the penetration of external hydrogen into the crystal lattice, creating interstitial or substitutional solid solutions. In turn, plastic deformation contributes to creating new crystal lattice defects deep inside the bulk metal. The atomic external interstitial hydrogen, moving along the crystal lattice, finds nano- and micropores, wherein it collects mollies and creates an excess pressure gradient, which contributes to the destruction of the metal.

It promotes the penetration of external hydrogen into alloyed cast iron by its thermal expansion. As a result of exposure to high temperatures within small limits, the piston rings change their diameter due to an increase in the intermolecular distance of atoms in the crystal lattice. This leads to the fact that the outer atomic hydrogen, which has the smallest size of all known chemical elements, encounters fewer obstacles on the way from the surface to the depths of the rings.

As an indicator of the degree of external hydrogen diffusion into the crystal lattice of a solid, one can use a criterion based on the Knudsen number k, x_o $K_n = \frac{\lambda}{L}$, where λ is the average free path of molecules in a gas, and L is the characteristic size of the section.

The mean free path of a molecule is the length that a molecule travels from one collision to the next. In our case, the mean free path of a molecule is understood as the length that a molecule travels before colliding with an imaginary wall formed by two neighboring molecules. Therefore, the mean free path of a molecule is

$$\lambda = \frac{1}{\sqrt{2}\sigma_n} \tag{1}$$

where σ is the gas-kinetic effective cross-section of the molecule, and n is the concentration of molecules.

The gas-kinetic effective cross-section of a molecule in the case of scattering with allowance for temperature and pressure gradients is

$$\sigma = \sigma_0 \left(1 + \frac{S \cdot P_H}{gradT \cdot gradP} \right). \tag{2}$$

where σ_0 is the depth of the potential well; P_H is the pressure of the counterbody per unit area of the body, MPa; S is Sutherland's constant ($S_{H2} = 72$); and K, $gradT$, and $gradP$ are the gradients of temperature and pressure on the body surface.

The characteristic cross-sectional size L for bodies can be determined from the parameters of the crystal lattice, taking into account the fact that the piston rings are made of high-strength nodular cast iron (Figure 1) with inclusions of graphite (which belong together with molybdenum disulfides and diselenides, and gallium and indium monoselenides) to the family of 2D layered materials with their unique properties [24–32]. On the lattice scale, the distance between graphite layers intercalated by hydrogen (up to 75 ppm and possibly by short-length hydrocarbons) [33] is equal to 0.335 nm, can be taken as the characteristic size of the section, and is the ideal gap (due to low van der Waals interaction between the layers) for the hydrogen intercalation process and the formation of the hydrogen nanocontainer [16]. In the hydrogen-containing (up to 12 ppm) and hydrogen-accumulated (in a nanocontainer) (up to 600 ppm) lubricant-cooling (liquid, solid, gaseous) environment application, hydrogen enters the near crack initiation contact zone before fracture. It takes part in changing structural material fracture mechanisms. Behind the unique mechanical properties, layered materials also demonstrate excellent electronic characteristics. Van der Waals heterostructures of graphene/InSe/graphene electrodes, spaced by an InSe nanolayer of c.a. 20–30 nm thickness, manifest high photosensitivity at room temperature. In combination with transparent conductive graphene, these structures can be used for 2D electronics and optoelectronics. Record figures of merit for the layered materials have been observed in carriers' mobility, optical sensitivity, catalytic hydrogen generation, and reversible hydrogen storage [24–29]. It has been established that ultrathin

InSe layered materials possess several unique properties that qualitatively distinguish them from other graphene-like two-dimensional crystals. Namely, the possibility of reversible intercalation, i.e., in-situ band tuning, is a valuable tool for hydrogen evolution reactions and hydrogen storage.
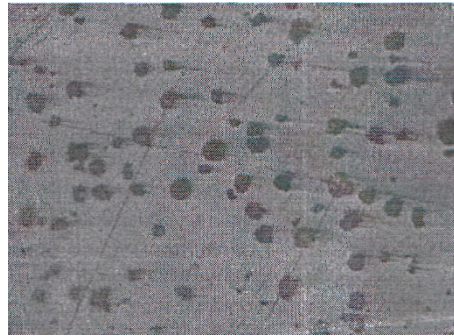

Figure 1. Typical structure of nodular cast iron.

The concentration of external hydrogen molecules in the friction zone is mainly driven by a dissociation process of hydrocarbon fuel and lubricant.

It is known that during the operation of piston rings, intense hydrogen wear occurs, and the concentration of hydrogen molecules released from the fuel and lubricant exceeds the concentration of hydrogen molecules inside the piston rings, which leads to the formation of a concentration gradient *gradC*.

Then, taking into account the above dependencies, we estimate:

$$K_n = \frac{1}{L}\left[2\sigma_0 \cdot gradC\left(1 + \frac{S \cdot P_H}{gradT \cdot gradP}\right)\right]^{-1/n}. \tag{3}$$

The alloying elements may also react by forming a chemical compound with internal hydrogen. Thus, with a decrease in the concentration of biographical hydrogen in the metal, a hydrogen wear reduction occurs despite the supply of external hydrogen quantities from the fuel mixture and lubricant. The direction and rate of hydrogen diffusion are determined by the temperature in the friction zone, which reaches its highest values at a certain depth from the surface; elastic and plastic deformations in the friction zone, which, as a consequence, causes the dislocations to climb; and vacancies and collectors, where external hydrogen creates high pressure, thereby accelerating the destruction of the metal. In this case, the effect of the material structure is limited by the size of each phase's crystal lattice, which affects the diffusion rate accordingly. The source of hydrogen is hydrogen batteries based on intermethalides and composite materials, which provide a sufficient amount of hydrogen for long-term use during treatment of difficult-machined materials, which possess high fracture toughness, durability, and other unique properties: Mg_2NiH_2, MgH_2, TiH_x, and $Ti_2Ni(H_x)$ for high-speed steels and Ti_2NiH_x, Ti_2NiH_x, (Ti-Mg)-H, and TiFe for hard alloys [19]. These types of materials include hydrogen intercalated layered alloys [19] (Figure 2). During gas saturation, the crystal absorbs up to 400 ppm hydrogen, the main part of which spatially is distributed inside the van der Waals gap, forming a hydrogen-containing "nanobelt" with a thickness of several nm. Then, after six months of exposure at ambient conditions, the hydrogen concentration is c.a. 0.012 m.% (hydrogen mainly leaves the "embodiment" position directly in the matrix layer, and the crystal desorbs the diffusion active moving hydrogen). By electrolytic deposition, the hydrogen concentration can surpass the 600 ppm level immediately after saturation; however, it localizes in the van der Waals gap within the surface area, whereas during saturation from the gas phase, it is distributed throughout the entire volume (Figure 2).
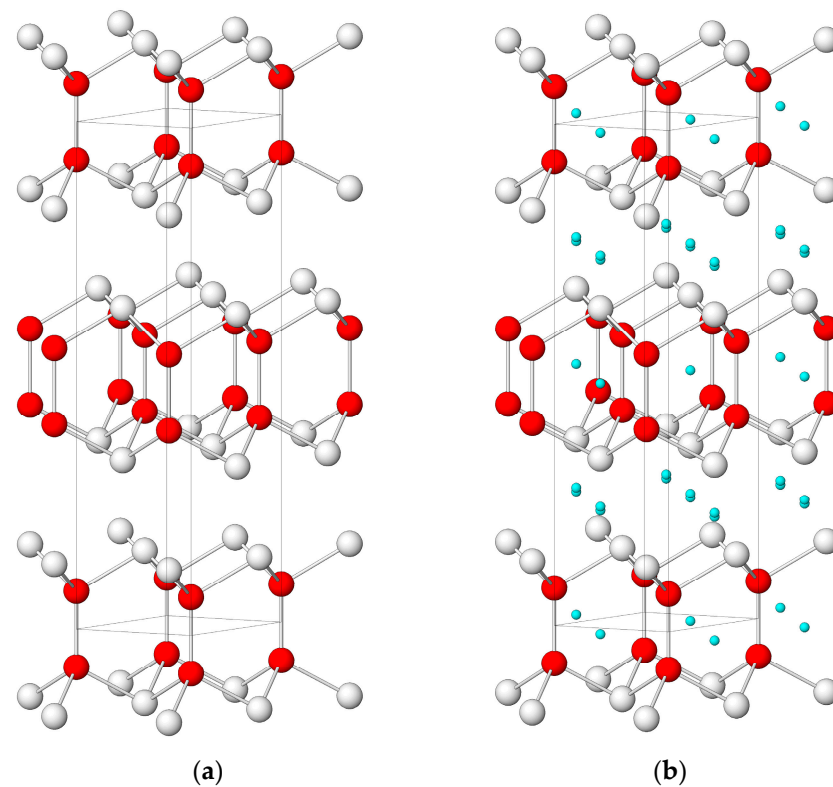
(**a**)   (**b**)

Figure 2. A typical unit cell of layered graphite-like materials (gallium (indium) monoselenides) before (**a**) and after hydrogen penetration into the crystal layer (proton—•) and in the interlayer (molecules—••) spaces (hydrogen nanocontainer) (**b**).

The absorption of hydrogen by layered crystals is more intense than that of oxygen. It is manifested in the abnormal displacement of the exciton absorption band in the layered InSe and GaSe crystals with an increasing degree of hydrogen intercalation. In the interlayer space of the crystal, hydrogen is in the molecular state (H_2), occupying translationally ordered places (pores).

As its concentration increases ($x > 2$), H_2 molecules dissociate and enter the matrix layers of the crystal in the form of ions [26,28,29]. Proton saturation describes the following reaction [30]:

$$Ga(In)Se + x\, H^+ + x\, e^- = H_x Ga(In)Se \qquad (4)$$
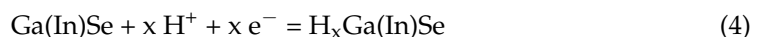
With the change in hydrogen concentration (in the $x = 0 \div 2.5$ range), the interlayer cell parameter *c* increases nonlinearly according to $c(x) \sim th(x)$ dependence. For the GaSe compound, the value of c increases from 1.589 (when $x = 0$) to 1.594 nm (when $x = 2.5$), and then a subsequent increase in the concentration of x alters this parameter only to 1.596 nm. The hydrogen forms a "nanoband," limited by the linear size of the crystallite and capable of reversible absorbing–releasing hydrogen cycles. Under the mentioned conditions, the absolute value of the change in the parameter c trends according to the thermal expansion mechanisms from room temperature to 373 K [28,29,31]. During hydrogen intercalation, the crystal lattice parameter *a* is also altered (from 0.375 to 0.377 nm).

For the InSe compound, due to hydrogen intercalation, the crystal lattice c parameter increases from 2.497 (when $x = 0$) to 2.504 nm (when $x = 1.5$), and with a further increase in concentration, it increases only to 2.506 nm. Similar to the InSe, during hydrogen intercalation, the parameter of the crystal lattice increases (from 0.3998 to 0.407 nm), which indicates the partial entry of ionized hydrogen (by the mechanism of "embodiment") into the layers of the crystal (Figure 2). The increase in the lattice parameters of gallium and indium monoselenides with increasing hydrogen concentration is accompanied by a weakening of the forces of interatomic bonds and the appearance of micro stresses

in the crystal lattice. The density of the studied crystals does not change significantly (ρ = 5.04 g/cm^3 for H$_2$GaSe and ρ = 5.61 g/cm^3 for H$_2$InSe).

Two states of hydrogen in the H$_x$GaSe compound are suggested [30]: "quasi-liquid," wherein it is localized in the van der Waals slit, and "bound," wherein ionized hydrogen penetrates the structure of layered packets, and during electrochemical incarnations in the matrix layers phase transitions occur with the achievement of specific values of x. At the initial stage, hydrogen molecules form a "quasi-liquid" film in the form of a nanoband in the van der Waals slit, and the proton magnetic resonance (PMR) spectral monolith has a small width.

The increase in x up to 5.16 is accompanied by the localization of hydrogen (intercalant) in potential wells, located in the centers of the triangles of the selenium planes on both sides of the van der Waals slit ("quasi-liquid" film becomes "more viscous"), which leads to a spectrum expansion PMR, which, due to small splits, has a complex structure [31]. Deformation stresses associated with introducing a significant amount of intercalated hydrogen cause more intense growth of elastic constants [34], which characterize the bond between hydrogen atoms in the interlayer space compared to the corresponding values directly in the matrix layer [29].

This fact is confirmed by the shift of the exciton maximum by 7 meV toward the region of higher energies in the range of hydrogen concentrations 0–0.4 and the increase in the bandgap (Eg) and the binding energy of the exciton (E$_{ex}$). The parameter Eg changes due to the competitive contribution of interlayer deformations and deformations within the layer, which has different signs of deformation potential [29]. Nuclear magnetic resonance (NMR) studies [28] combined with X-ray diffraction analysis indicate that at low values of x $\leq$ 1, the main contributor to the NMR spectrum is a band associated with molecular hydrogen in the interlayer space. Multiple cycles of intercalation–deintercalation do not impair the essential characteristics, and deintercalation in them for values of x $\rightarrow$ 4 can reach 90% of the amount of absorbed hydrogen.

Thus, hydrogen enters both the layered and interlayer spaces of the crystal (Figure 2). If x < 2, it is mainly located in the interlayer space, which is accompanied by an increase in the interlayer distance (and the crystal lattice parameter c). With a further increase in concentration (up to 5), it partially enters the layer space, where ion–covalent solid bonds act, leading to an increase in the crystal lattice parameter. Note that s-element ions can be introduced into InSe and GaSe crystals by electrochemical intercalation, and p- and d-elements are collected on the surface. During intercalation from aqueous solutions, the value potential (φ) is essential for reducing hydrogen ions.

For neutral solutions (pH7) φ = -0.41 V and if the cation of the salt solution is a metal whose standard electrode potential is much more positive than -0.41 V, a metal (Ag, Cu, Tl, Co) will be released at the cathode.

S-elements possess negative standard electrode potentials (for example, K, Ba, Ca, Na). Their positive ions, which accumulate in the near-cathode space under the action of an external electric field, have the opportunity to be embodied in the interlayer space of gallium and indium monoselenide crystals graphite and molybdenum diselenides [28,29]. Layered nanostructures and systems [28,29] can also be used as promising materials that accumulate hydrogen. Their efficiency depends on the reversible processes of "intercalation–deintercalation", i.e., the sorption–desorption properties of the van der Waals gap. For comparison, we note that the sorption capacity of the carbon nanotubes or nanobands used is due to the degree of filling (η_H) of the single-layer nanotube or nanoband with molecular hydrogen [5,31]:

$$\eta_H = \frac{\rho_H}{\rho_H + \rho_C} \approx \frac{0.07}{0.07 + \frac{30.4}{D}} \tag{5}$$

where ρH = 0.07 g/cm^3 is the density of hydrogen. At a diameter of D = 1.5 nm, the maximum degree of hydrogen filling $\eta H \approx$ 3.3 wt.%. The degree of filling ηH = 6.5 wt.% is achieved using nanotubes or nanobands larger than 3 nm in molecular containers for hydrogen storage.

A beam composed of single-layer nanotubes or nanobands can be considered a different type of hydrogen-containing nanostructure. The mass density of the beam (Table 1), consisting of similar nanostructures, depends on the maximum surface density of hydrogen ($2.56 - 10^{-9}$ g/cm^2) and the density of nanoformations. Filling the space between them gives a tangible result.

Table 1. Mass capacity of hydrogen in a beam of nanotubes of different diameters [5,31].

Diameter, nm	0.5	1	1.5	2	2.5	3
η_H, %	3.4	4.4	5.4	6.5	7.6	8.6

When mastering molecular containers, using beams of single-walled nanostructures with a cross-section of 1.2–1.5 nm with a distance between the surfaces of nanostructures of about 1 nm, you can achieve a hydrogen content of up to 11–12 wt.%. Thus, the absolute values of the tensile strength-layered materials oriented perpendicular to the c-axis (in the direction of the van der Waals bonds) are smaller than those directed parallel to the crystal layers. The introduced hydrogen (in an amount from 108 to 120 ppm) increases this difference by up to 30%. It may form adsorbed atoms or adatoms during the adsorption of external hydrogen on the surface of the piston rings (Figure 3). Considering the small size of the hydrogen molecule, thermal expansion of the rings, gradients of concentration, pressure, and deformation, the assumable number of formed adatoms is insignificant. In addition, during friction, the existence of a temperature gradient along the normal surface to the friction surface leads to the fact that external hydrogen will diffuse into the depth of the metal. It follows from this that the formation of hydrogen adatoms on the hydrogen wear of piston rings is small.
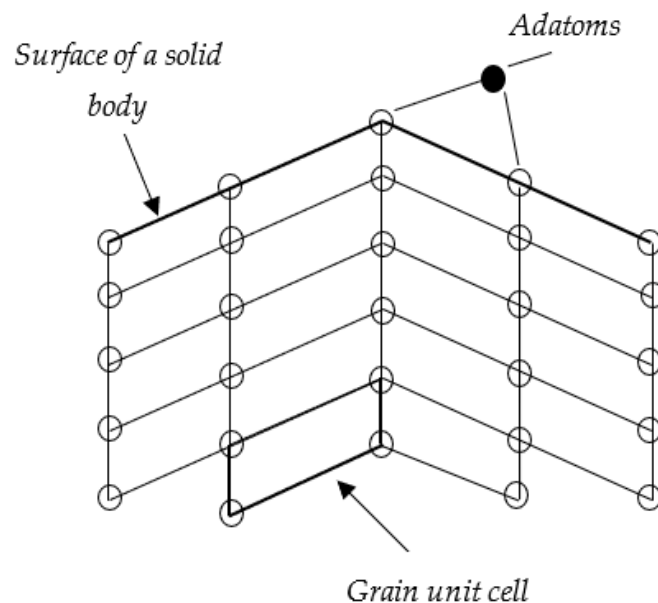

Figure 3. Formation of hydrogen adatoms at the crystal lattice boundary.

The effect of nano roughness of the surfaces of the piston rings and cylinder wall in reciprocating engines on hydrogen diffusion in the first approximation can be considered from the point of view of the structure of the crystal lattice [14].

Thus, it can be assumed that the main factors affecting the rate of hydrogen wear are temperature, pressure, deformations, structure, and crystal lattice defects (Figure 3). The general equation of the diffusion of hydrogen can be written as:

$$\frac{dq}{d\tau} = D_0 \frac{\partial C}{\partial x} + D_\xi \frac{\partial \xi}{\partial x} - D_T \frac{\partial T}{\partial x} \tag{6}$$

where D_0, D_{ξ}, and D_T are the coefficients of concentration, deformation, and temperature, respectively.

Based on this, it is possible to offer a generalization in Table 2.

Table 2. Stages of hydrogen wear of the friction pair "ring–cylinder mirror" working surfaces during electrothermomechanical friction.

Stages	Processes, Phenomena, and Effects Arising from the Action	
	Alternating Loading in Friction Couple	**Result**
1	Intensive release of hydrogen in the friction zone from decomposed lubricant.	Tribochemical reactions are intensified: When the rings slide against the cylinder, an electromagnetic field is created, which captures atomic hydrogen, directing it into microcracks.
2	Desorption of water from the cylinder surface.	The temperature of the friction surface rises.
3	Hydrogen adsorption by the working surface of the cylinder and piston ring materials.	Intensive diffusion of external hydrogen.
4	Diffusion of atomic hydrogen into the crystal lattice of the piston rings and the surface layers of the cylinder; their intensity is determined by the gradients of the surface and volumetric temperatures and equivalent stresses.	Combination of external hydrogen with carbon (C), which is present in the crystal lattice of the metal (Fe_3C); temperature gradients and mechanical-temperature stresses increase.
5	The hydrogen concentration in the subsurface layer with maximum temperature.	An increase in temperature gradients in the subsurface layer.
6	A. Low-temperature brittle fracture of the surface layer of metallic friction elements saturated with hydrogen as a result of the formation of a large number of microcracks on the cylinder surface.	The periodic occurrence of a traveling stress wave (tension–compression) enhances the saturation, with the hydrogen of the parts deformed by the friction of the near-surface volumes of the metal; equivalent stresses increase, hydrogen mobilization occurs.
	B. High-temperature viscous destruction of the rubbing layer of the rings in the form of spreading it on the surface of the cylinder mirror as a result of metal flow.	At temperatures of about 1073–1273 K, the metal surfaces of the rings are oversaturated with hydrogen.

3. Hydrogen Wear of Piston Rings of Engine Cylinders and Ways to Reduce It

Numerous studies [1–5,14–18,35,36] of hydrogen wear of the cylinder–piston group of internal combustion engines have shown the dominant role of both technological (internal) and operational (external hydrogen) in the wear of piston rings. The determination of the content of hydrogen in the parts was carried out by vacuum extraction. When the friction couple "cylinder–piston ring" operates, there is a cyclic change in loads at high temperatures and specific loads (3000 K, 10–12 MPa in compression–ignition engines, 5.5 MPa in spark-ignition engines). Such operating conditions lead to thermomechanical destruction of the working medium with the formation of free (external) hydrogen and its subsequent adsorption by the rubbing surfaces of the cylinders and piston rings. A traveling stress wave (tension–compression) periodic occurrence enhances the hydrogen saturation of near-surface metal volumes during friction. It is believed that less hydrogen increasing the wear life of the rings are the material fracture mechanics parameters. We take into account the material's wear resistance. If the rings are made of different materials, then it is necessary to determine the electrothermal layer arising on the working surface and take into account their mechano-physical properties.

The studies carried out have shown that the piston rings of D-50, D-240, ZMZ-24, CC-10UD, etc. engines are primarily susceptible to both technological and operational hydrogen saturation. Tables 3 and 4, and Figures 2 and 3 show the content of diffusion-active hydrogen in the piston rings [5].

Table 3. The hydrogen concentration in piston rings.

Ring Position	Engine and Coating Type			
	PD-10UD	D-50	D-240	ZMZ-24
	Chromium			Molybdenum
	Porous		Hard	
	Hydrogen Concentration C_H, ppm			
Top	$\frac{38.1}{2.67} = 14.3$	$\frac{16.0}{2.34} = 6.83$	$\frac{8.46}{1.95} = 4.33$	$\frac{18.5}{5.12} = 3.61$
Bottom, tin-coated				

Table 4. The hydrogen concentration in piston rings depending on their position.

No	Manufacturer	Ring	C_H, ppm	Coating
1	"Riken" (Japan)	Top Bottom	$\frac{5.24}{1.43} = 3.7$	Hard chromium Phosphating
2	"Nippon" (Japan)	Top Bottom	$\frac{8.57}{2.14} = 4.0$	Hard chromium Ferrox
3	"Teikoku" (Japan)	Top Bottom	$\frac{13.1}{5.1} = 2.56$	Phosphating Porous chromium
4	"Getz" (Germany)	Top Bottom	$\frac{13.8}{5.0} = 2.64$	Phosphating Porous chromium

Data analysis of Tables 3 and 4 shows the following when using different materials for rings located at different positions on the piston:

- The maximum ratio of the concentration of internal hydrogen is achieved for the porous chromium ring material and the minimum for the molybdenum material, and the bottom ring was tinned;
- The ratio of the concentration of internal hydrogen for rings made of porous chromium used in various engines is questionable.

As for Table 3, the following can be deducted:

- The maximum ratio of the concentration of internal hydrogen is achieved for the materials of rings with different coatings for the Nippon manufacturer rings, and the minimum for the Teikoku rings;
- A significant decrease in the concentration of hydrogen is achieved due to various types of coatings of piston rings, compared to rings without coatings;
- In comparison to the maximum hydrogen absorption (different for different structural materials), in the case of low hydrogen absorption, the wear resistance of the rings increases by 20–25%.

The piston rings of the Raba–Mann engine during operation (Ikarus, Budapest and Székesfehérvár, Hungary) are characterized by the concentration of diffusion-active external hydrogen increases by almost 9.4 times (from 1.46 to 13.66 ppm). It has been established that various technological operations on the surface of the rings have a different effect on the processes of hydrogen absorption.

To protect metals from the effects of hydrogen at elevated temperatures and pressures, the following recommendations are elaborated: the introduction of strong carbide-forming elements (chromium, molybdenum, vanadium, niobium, titanium) into steel to stabilize the carbide component and prevent the steel from decarburization, and cladding or lining the steel with metals with a lower hydrogen permeability (for example, copper, silver, aluminum, steel 0.08C13Cr or 0.12C18Cr10NiTi, etc.) [3]. The existing steel can be recommended to have a particular structure. Soft coatings on the rings will not last long. They need to be reinforced with nanomaterials. It is known that the presence of alloying elements

in the structure of cast iron and steel, such as manganese, chromium, tin, molybdenum, and some others, reduce hydrogen permeability and, consequently, hydrogen wear [3,37,38].

It has been established that the transfer of heat during electrothermomechanical friction during its accumulation on the surface layer of the metal friction element occurs along the normal surface from places with a higher temperature to areas with a lower temperature. In this case, a surface temperature gradient arises. The most significant deep temperature drop occurs in the direction of the normal surface to the area of the contact spot of the micro-protrusion (Figure 4 shows the interaction of two surfaces and the direction of the unit vectors coinciding with the direction of the normal surface to the unit contact area). In general, the specific direction of the normal surface n to the contact does not coincide with the unit vectors. Propagating deep into the material, the temperature field leads to a change in its mechanical properties in a thin surface layer. The magnitude of the heat flux depends on friction and the size of the area on which it accumulates.
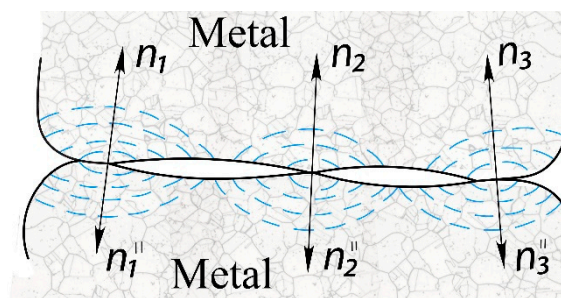

Figure 4. The contact of two rough surfaces.

Let us consider the unsteady temperature problem of friction. Imagine a metal bar of a rectangular cross-section pressed by the specific load p against the surface of a rotating disk (Figure 5).
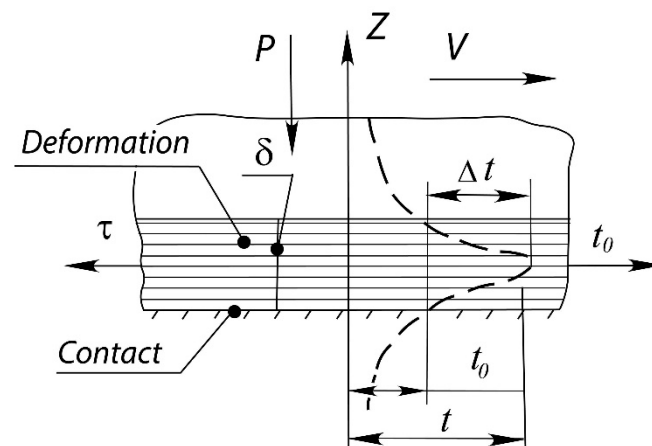

Figure 5. The change in temperature t along the normal surface z to the friction surface (in the deformed surface layer) of metallic friction element: layer (t); initial (t_H); increments (Δt); environment (t_0); shear stresses (τ); surface layer (δ); sliding speed (v); and z—the origin of the coordinate axis is located on the middle surface of the layer.

In this case, it is assumed that the disc material has higher strength, and plastic deformations occur in the surface layer of the rod, which are the same in thickness. Therefore, the temperatures of the planes bounding the surface layer are equal to each other. If there is no polymorphism (no changes in the type of crystal lattice) face-centered cubic (FCC), body-centered cubic (BCC), and hexagonally close-packed (HCP) crystal structures are possible depending on specific loads and surface-bulk temperature—the latter impact the

subsurface and subsurface layer of the metallic friction element. If we consider the model of solid layers, then in the first case, the layers remain close-packed (CP), but move away from each other. In the second, the atoms of neighboring layers touch each other, but a gap appears between the atoms in the layer itself, and therefore all actual HCP structures are not genuinely closed-packed.

In reality, however, the difference in c/a (where c and a are the height and width of the cube ribs, respectively) is variable c/a <1.633 (1.633 is the ideal value), meaning that the atoms in HCP metals are not spherical, but ellipsoids (compressed balls with the ratio in planes of $1.633 < c_h/a_v > 1.633$). Thus, under the action of impulse-specific loads in friction pairs of "metal–metal in piston rings," the atoms in the layers, as well as the layers themselves, are compacted, which contributes to the accumulation of energy in them due to the high electrothermal resistance, and as a consequence, an increase in the surface-bulk temperature.

For example, silicon is one of the elements that effectively reduces hydrogen permeability. Silicon has forms carbides. Consequently, if silicon molecules are introduced into the crystal lattice structure, it is possible to obtain carbides at a certain depth from the metal surface. However, in this case, several shortcomings arise, namely, splitting powdered silicon into molecules, an increase in the parameters of the crystal lattice of cast iron or steel to the point-wise direction of silicon molecules into it, and occupation by silicon molecules of vacancies in the crystal lattice, and as a consequence, carbidization of the subsurface structure of the metal.

Thus, it is necessary to form a barrier for external hydrogen from friction couples at the nano and micro levels to increase their wear resistance. The cost-effectiveness of the presented approach can be benefited within a few months of the operational timeframe. The service life may be extended significantly by removing hydrogen from the piston rings, i.e., reducing the heterogeneity of the structure, residual stresses, and uneven physico-chemical properties of the subsurface layers, which reduces the stress concentration and, consequently, improves the functional properties of the friction pair surface of "cylinder–piston rings" in the diesel engine. This leads to savings while increasing the durability of the materials used in connection with the time between repairs.

4. Conclusions

The relationship between external and internal (biographical) hydrogen in "cylinder–piston ring" friction couples in spark ignition engines has been established. The hydrogen wear of the piston rings is estimated, and strategies for its reduction are elucidated. Under the influence of high temperatures and pressure, the oil in the combustion chamber at a temperature up to 1473 K decomposes and forms small amounts of water, from which external hydrogen (H_2) is subsequently formed.

During friction, the existence of a temperature gradient along the normal surface to the friction surface leads to the fact that external hydrogen will diffuse into the depth of the metal. It has been described that the external and internal hydrogen interaction in the "cylinder–piston rings" friction couple performs unequal work of friction with a minority of surfaces mutually overlapping.

Layered nanostructures and systems (graphite inclusions in nodular cast iron) can be considered materials that effectively accumulate hydrogen. Their efficiency depends on the reversible processes of intercalation–deintercalation, i.e., the sorption–desorption properties of the van der Waals gap. Hydrogen removal from piston rings reduces the heterogeneity of the structure, residual stresses, and uneven physical and chemical properties of the near-surface layers, which reduces the stress concentration and, as a consequence, leads to an improvement in the performance characteristics of the surface layers of the friction couple "cylinder–piston rings" in spark ignition engines.

References

1. Balyts'kyi, O.I.; Chmiel, J.; Krause, P.; Niekrasz, J.; Maciag, M. Role of hydrogen in the cavitation fracture of 45 steel in lubricating media. *Mater. Sci.* **2009**, *45*, 651–654. [CrossRef]
2. Balyts'kyi, O.I.; Abramek, K.F.; Mruzik, M.; Shtoeck, T.; Osipowicz, T. Evaluation of the losses of hydrogen-containing gases in the process of wear of pistons of an internal-combustion engine. *Mater. Sci.* **2017**, *53*, 289–294. [CrossRef]
3. Kindrachuk, M.V.; Vol'chenko, D.A.; Vol'chenko, N.A.; Stebeletskaya, N.M.; Voznyi, A.V. Influence of hydrogen on the wear resistance of materials in the friction couples of braking units. *Mater. Sci.* **2017**, *53*, 282–288. [CrossRef]
4. Dmytrakh, I. Corrosion fracture of structural metallic materials: Effect of electrochemical conditions in crack. *Strain Int. J. Exp. Mech.* **2011**, *47*, 427–435. [CrossRef]
5. Suranov, G.I. *Hydrogen: Fracture, Wear, Lubrications of Machine Parts*; UTU: Uchta, Russia, 2015; 224p.
6. Rovin, L.E.; Zayac, T.M.; Valickaya, O.M. Recycling of ferrous metal shavings. *Cast. Metall.* **2017**, *89*, 94–101. [CrossRef]
7. Myshkin, M.I.; Petrokovets, N.K. Friction, lubrication and wear. In *Physical Foundations and Technical Applications of Tribology*; Fiz-matlit: Moscow, Russia, 2007; 368p.
8. Balyts'kyi, O.I.; Abramek, K.F.; Shtoeck, T.; Osipowicz, T. Diagnostics of degradation of the lock of a sealing ring according to the loss of working gases of an internal combustion engine. *Mater. Sci.* **2014**, *50*, 156–159. [CrossRef]
9. Brunhart, M.; Soteriou, C.; Daveau, C.; Gavaises, M. Cavitation erosion risk indicators for a thin gap within a diesel fuel pump. *Wear* **2020**, 203024. [CrossRef]
10. Yudin, V.M.; Lukashev, E.A.; Stavrovsky, M.E. *Tribochemistry of Hydrogen Wear*; MGUPS: Moscow, Russia, 2004; 282p.
11. Liu, D.; Bai, B.; Fang, H.; Zhang, W.; Gu, J.; Chang, K. Effect of temperature and carbide free bainite on the mechanical characteristics of a high strength-low alloy steel. *Mater. Sci. Eng. A* **2004**, *371*, 40–44. [CrossRef]
12. Deulin, E.A.; Michailov, Y.V.; Panfilov, R.A. *Mechanics and Physics of Precise Vacuum Mechanisms*; Springer: New York, NY, USA, 2012; 234p.
13. Pashechko, M.; Jozwik, J.; Dziedzic, K.; Usydus, I. Surface hardening of HS6-5-2 quick-cutting steel in the course of chemical thermal treatment. *Mater. Sci.* **2017**, *52*, 834–840. [CrossRef]
14. Simon, L.; Moraes, C.A.M.; Modolo, R.C.E.; Vargas, M.; Calheiro, D.; Brehm, F.A. Recycling of contaminated metallic chip based on eco-efficiency and eco-effectiveness approaches. *J. Clean. Prod.* **2017**, *153*, 417–424. [CrossRef]
15. Weber, U.; Deimel, P.; Saraev, D.; Sattler, E.; Schmauder, S.; Soppa, E. Influence of hydrogen on the deformation behavior of a ferritic fine-grained low alloy steel. *Comput. Mater. Sci.* **2005**, *32*, 577–587. [CrossRef]
16. Holubets, V.M.; Pashechko, M.I.; Dzedzic, K.; Borc, J.; Tisov, A.V. Frictional strength of electric spark coatings from powder wires under friction without lubrication. *J. Frict. Wear* **2020**, *41*, 443–446. [CrossRef]
17. Pashechko, M.; Montusiewicz, J.; Dziedzic, K.; Jozwik, J. Multicriterion assessment of wear resistance of Fe–Mn–C–B eutectic coatings alloyed with Si, Ni, and Cr. *Powder Metall. Met. Ceram.* **2017**, *56*, 316–322. [CrossRef]
18. Jozwik, J.; Dziedzic, K.; Barszcz, M.; Pashechko, M. Analysis and comparative assessment of basic tribological properties of selected polymer composites. *Materials* **2020**, *13*, 75. [CrossRef]
19. Balitskii, O.A.; Kolesnikov, V.O.; Balitskii, A.I.; Eliasz, J.J.; Havrylyuk, M.R. Hydrogen effect on the high-nickel surface steel properties during machining and wear with lubricants. *Arch. Mater. Sci. Eng.* **2020**, *104*, 49–57. [CrossRef]
20. Balitskii, O.A.; Kolesnikov, V.O.; Balitskii, A.I. Wear resistance of hydrogenated high nitrogen steel at dry and solid state lubricants assistant friction. *Arch. Mater. Sci. Eng.* **2019**, *98*, 57–67. [CrossRef]

21. Balyts'kyi, O.I.; Krokhmal'nyi, O.O. Pitting corrosion of 12Kh18AG18Sh steel in chloride solutions. *Mater. Sci.* **1999**, *35*, 389–394. [CrossRef]

22. Akid, R.; Dmytrakh, I.M.; Gonzalez-Sanchez, J. Fatigue damage accumulation: The role of corrosion on the early stages of crack development. *Corros. Eng. Sci. Technol.* **2006**, *41*, 328–335. [CrossRef]

23. Michelich, J.L.; Troiano, A.R. Delayed failure in hydrogenated facecentred cubic alloy in nickel. *Nature* **1963**, *197*, 996–997. [CrossRef]

24. Bandurin, D.A.; Tyurnina, A.V.; Geliang, L.Y.; Mishchenko, A.; Zólyomi, V.; Morozov, S.V.; Kumar, R.K.; Gorbachev, R.V.; Kudrynskyi, Z.R.; Pezzini, S.; et al. High electron mobility, quantum Hall effect and anomalous optical response in atomically thin InSe. *Nat. Nanotechnol.* **2017**, *12*, 223–227. [CrossRef] [PubMed]

25. Warren, S.C.; Voïtchovsky, K.; Dotan, H.; Leroy, C.M.; Cornuz, M.; Stellacci, F.; Hébert, C.; Rothschild, A.; Grätzel, M. Identifying champion nanostructures for solar water-splitting. *Nat. Mater.* **2013**, *12*, 842–849. [CrossRef]

26. Felton, J.; Blundo, E.; Ling, S.; Glover, J.; Kudrynskyi, Z.R.; Makarovsky, O.; Kovalyuk, Z.D.; Besley, E.; Walker, G.; Polimeni, A.; et al. The interaction of hydrogen with the Van der Waals crystal γ-InSe. *Molecules* **2020**, *25*, 2526. [CrossRef] [PubMed]

27. Mudd, G.W.; Svatek, S.A.; Hague, L.; Makarovsky, O.; Kudrynskyi, Z.R.; Mellor, C.J.; Beton, P.H.; Eaves, L.; Novoselov, K.S.; Kovalyuk, Z.D.; et al. High broad-band photoresponsivity of mechanically formed InSe-graphene Van der Waals heterostructures. *Adv. Mater.* **2015**, *27*, 3760–3766. [CrossRef] [PubMed]

28. Zhirko, Y.I.; Kovalyuk, Z.D.; Trachevsky, V.V.; Melnik, V.V. NMR investigations of hydrogen intercalates in GaSe layered crystals. *NATO Sci. Ser. Environ. Secur.* **2012**, *2*, 443–458. [CrossRef]

29. Kaminskii, V.M.; Kovalyuk, Z.D.; Pyrlya, M.N.; Gavrilyuk, S.V. Properties of hydrogenated GaSe crystals. *Inorg. Mater.* **2005**, *41*, 793–795. [CrossRef]

30. Dmytrakh, I.M.; Leshchak, R.L.; Syrotyuk, A.M.; Barna, R.A. Effect of hydrogen concentration on fatigue crack growth behaviour in pipeline steel. *Int. J. Hydrog. Energy* **2017**, *42*, 6401–6408. [CrossRef]

31. Wang, J.; Wang, L.; Ma, L.; Zhao, J.; Wang, B.; Wang, G. Structures, electronic properties, and hydrogen-storage capacity of single-walled TiO_2 nanotubes. *Phys. E Low Dimens. Syst. Nanostructures* **2009**, *41*, 838–842. [CrossRef]

32. Ubbelohde, A.R. Anisotropy of synthetic metals. *Nature* **1971**, *232*, 43–44. [CrossRef] [PubMed]

33. Yoshimoto, T.; Matsuo, T.; Ikeda, T. The effect of graphite size on hydrogen absorption and tensile properties of ferritic ductile cast iron. *Procedia Struct. Integr.* **2019**, *14*, 18–25. [CrossRef]

34. Balyts'kyi, O.O. Elastic characteristics of laminated gallium and indium chalcogenides. *Mater. Sci.* **2004**, *40*, 706–709. [CrossRef]

35. Prajwowski, K.; Golebiewski, W.; Lisowski, M.; Abramek, K.F.; Galdynski, D. Modeling of working machines synergy in the process of the hybrid electric vehicle acceleration. *Energies* **2020**, *13*, 5818. [CrossRef]

36. Jamrozik, A.; Tutak, W.; Grab-Rogalski, K. Combusting stability, performance and emission characteristics of a CI engine fueled with diesel/n-butanol blends. *Energies* **2021**, *14*, 2817. [CrossRef]

37. Fominski, V.Y.; Romanov, R.I.; Fominski, D.V.; Novikov, S.M.; Chesnokov, A.V. Features of sliding friction on thin-film Mo–S–C coatings prepared by pulsed laser deposition. *J. Frict. Wear* **2020**, *41*, 18–24. [CrossRef]

38. Osenin, Y.I.; Antoshkina, L.I.; Bugaenko, V.V.; Krivosheya, Y.V.; Chesnokov, A.V. The noise-generating mechanism during the application of disc brakes on rolling stock. *J. Frict. Wear* **2020**, *41*, 178–182. [CrossRef]